Journal of Biomolecular Structure & Dynamics, ISSN 0739-1102
Volume 18, Issue Number 5, (2001)

A Nanosecond Molecular Dynamics Study of Antiparallel $d(G)_7$ Quadruplex Structures: Effect of the Coordinated Cations

Shibasish Chowdhury and Manju Bansal*
Molecular Biophysics Unit,
Indian Institute of Science,
Bangalore-560012, India

http://www.adeninepress.com

Abstract

Nanosecond scale molecular dynamics simulations have been performed on antiparallel Greek key type $d(G_7)$ quadruplex structures with different coordinated ions, namely Na^+ and K^+ ion, water and Na^+ counter ions, using the AMBER force field and Particle Mesh Ewald technique for electrostatic interactions. Antiparallel structures are stable during the simulation, with root mean square deviation values of ~1.5 Å from the initial structures. Hydrogen bonding patterns within the G-tetrads depend on the nature of the coordinated ion, with the G-tetrad undergoing local structural variation to accommodate different cations. However, alternating *syn-anti* arrangement of bases along a chain as well as in a quartet is maintained through out the MD simulation. Coordinated Na^+ ions, within the quadruplex cavity are quite mobile within the central channel and can even enter or exit from the quadruplex core, whereas coordinated K^+ ions are quite immobile. MD studies at 400K indicate that K^+ ion cannot come out from the quadruplex core without breaking the terminal G-tetrads. Smaller grooves in antiparallel structures are better binding sites for hydrated counter ions, while a string of hydrogen bonded water molecules are observed within both the small and large grooves. The hydration free energy for the K^+ ion coordinated structure is more favourable than that for the Na^+ ion coordinated antiparallel quadruplex structure.

Introduction

In presence of alkali cations, DNA oligomers containing one or more contiguous guanine stretches form a family of higher order helical structures (1,2). Such guanine rich stretches occur at the eukaryotic chromosomal termini (3-6), immunoglobulin switch regions of higher organisms (7), mutation hotspots associated with human diseases (8), "CpG" islands located in the coding and promoter regions of genes (9), HIV-1 genomic RNA (10) and in triplet repeat sequences associated with fragile X syndrome (11). In presence of various cations, guanine rich sequences can adopt planer G-quartets alignment (Figure 1) with adjacent G-quartets stacking on each other to form G-quadruplex structures. In addition, proteins have been identified that specifically recognize these quadruplex-forming guanine rich sequences (9,12-17). The identification of these proteins provides evidence for the presence of quadruplex DNA *in vivo*. Earlier fibre diffraction studies (18,19) have successfully modeled the quadruplex structures which are stabilized by stacked guanine bases, while recent X-ray crystal structures (20,21) clearly demonstrate the formation of four-stranded quadruplex structures. The stability of quadruplex structures is known to be highly dependent on the favourable π-electron interactions between the stacked guanine bases and coordination of metal ions with exocyclic carbonyls. X-ray crystallographic studies have shown such coordination for K^+ ions in dimeric Greek key type antiparallel G-quadruplex (20) and Na^+ ions in tetrameric parallel G-quadruplex (21). Conformational polymorphism in guanine quadruplex structures has been suggested by earlier theoretical studies (22-24).

*Phone: +91-80-309-2534;
Fax: +91-80-3600683, +91-80-3600535;
Email: mb@mbu.iisc.ernet.in.

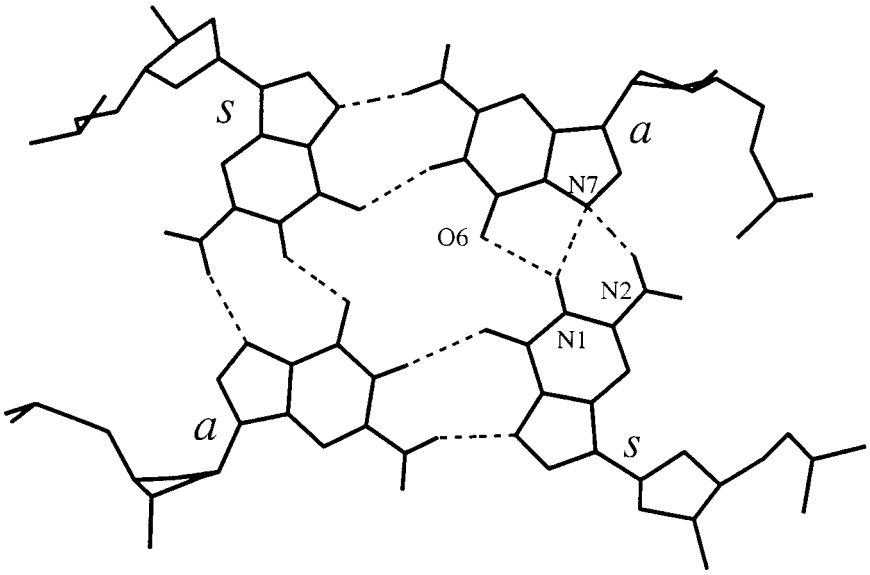

Figure 1: A down the helix view of a representative G-tetrad in the Greek key type antiparallel crystal structure (20) of d($G_4T_4G_4$) sequence. The alternating *anti-syn-anti-syn* glycosidic orientation is clearly seen. Dotted lines represent the hydrogen bonds, for which hydrogen to acceptor atom distance is < 2.6 Å, with the relevant acceptor atoms on strand 1 and donor atoms in strand 2 being indicated.

Crystal Structure

Oligonucleotides with short single contiguous guanine stretch favor the formation of parallel stranded intermolecular structures (25-31) and multiple contiguous guanine stretches can form antiparallel structures either by dimerization of hairpin duplexes (25,28,29,32,33) or by intramolecular folding of a single strand (34-36). However, there are significant differences among the different antiparallel quadruplex structures. For example, in nmr structure (33) the thymine loop is across the diagonal of the end quartets, while in the crystal structure (20) the loop is across the wide grooves, connecting the adjacent strands. This leads to adjacent strands being alternately parallel and antiparallel in nmr structure and adjacent strands being antiparallel in crystal structure (termed as Indian key and Greek key structures respectively). However, earlier molecular mechanics studies (22) have demonstrated that the G-stem of both the structures are energetically comparable, even though the size of the quadruplex grooves are different in the Indian and Greek key structures. Several physicochemical and nmr studies have demonstrated that topology of different quadruplexes depend upon ionic concentration and size of different cations (28,29,37-41). A structural explanation has been proposed for the large differences in the stability of the quadruplex formed by specific cations. The ion which is smaller than the quadruplex cavity, would not bind tightly the keto oxygens of guanines (5) or it may disrupt the quadruplex structure by pulling the oppositely charged O6 atoms into a partially vacant central cavity while larger cation may cause the steric disruption of hydrogen bonds between the strands (42). It is also observed that nmr spectrum of NaCl stabilized quadruplexes differs significantly from KCl stabilized quadruplexes (39,41,43). The nmr and thermodynamic studies demonstrated that if the cations are trapped inside the quadruplex cavity, their binding behavior and dynamic motion are different from externally bound counter ions and the various cations also behave differently (44-47). Recent molecular dynamics (48-50) and ab initio (51) studies have also demonstrated the effect of coordinated ion on quadruplex structure, particularly on G-tetrad geometry.

In order to understand the inherent stability and dynamics of G-quadruplexes, we have carried out nanosecond scale molecular dynamics (MD) simulations on both parallel and antiparallel, Greek key type, 7-mer quadruplexes, which constitute about half a turn of the quadruplex structure. Longer G-fragment helps in eliminating the artifacts due to end effects during the MD simulation and it also mimics longer G-rich triplet repeat sequences associated with disease (11). We chose to carry out simulations with Greek key type antiparallel quadruplex structure since this type of antiparallel structure is observed by X-ray crystallography (20). It is

worth noting that the stem part of both Greek and Indian key type quadruplex structures are energetically comparable (22). Coordinated Na^+ or K^+ ions were positioned between the G-tetrads and the quadruplex was surrounded by water molecules containing Na^+ counter ions. A 1.1 ns of MD simulation at 300K was followed by 1 ns at 400K to study the effect of elevated temperature on the structures. During the MD, detail structural analysis, tetrad stacking energy, hydration pattern and ion behaviour have been monitored for the various quadruplex structures. The analysis of the parallel quadruplex structure has been reported earlier (49,52). Here we describe the structural details for the antiparallel quadruplexes and compare them with that for the parallel structures.

Methods

The initial 7-mer Greek key type antiparallel quadruplex structure of poly d(G) was generated using the procedure described in our earlier paper (22). These quadruplex structures are having antiparallel adjacent strands with alternating *syn-anti* arrangement of bases along a chain as well as in the tetrad. Six K^+ or Na^+ ions were placed between the seven G-tetrads, as observed in the X-ray crystal structure of parallel quadruplex (21). The actual ion position was at the center of the twisted cube formed by eight keto oxygens of two-stacked guanine tetrads. The 7-mer quadruplex structures were surrounded by additional 24 Na^+ counter ions. The counter ions were placed 6 Å from each of the phosphorus atoms, along the bisector of the two pendant oxygens, using the EDIT module of AMBER. In each system, DNA, coordinated ions and counter ions were then placed in a pre-equilibrated box of TIP3P (53) water molecules and the periodic box of water was extended to a distance of 5 Å from DNA and counter ions giving an effective cylinder of 10 Å thickness around the quadruplex. Both the systems consisted of the 7-mer antiparallel quadruplex DNA, 6 coordinated Na^+ or K^+ ions, 24 Na^+ counter ions and 1530 water molecules with initial box dimension of 35.7Å × 43.8Å × 44.0Å. In all subsequent discussion, the system with Na^+ ion coordinated antiparallel structure is denoted as AP-Na whereas AP-K denotes the K^+ ion coordinated antiparallel structure. The net residual charge in the simulation box was neutralized using the option provided in AMBER. Molecular dynamics simulations were performed in the isothermic isobaric ensembles (P = 1 atm, T = 300 K) with SANDER module of AMBER 4.1 program (54) using the PARM 94 all atom force field and Particle Mesh Ewald method (PME) was used for the calculation of electrostatic interactions (55). This is a fast implementation of the Ewald summation method for calculating the full electrostatic energy of a unit cell in a macroscopic lattice of repeating images. PME has been successfully utilized in nanoseconds dynamics of highly charged DNA and RNA molecules (56-58). PME-MD method has been also used in several DNA simulations to understand other DNA structures and solvent behaviour around the DNA molecules (59-62). The PME grid spacing was ~1.0 Å. It was interpolated on a cubic B-spline, with the direct set tolerance set to 0.000001. Periodic boundary conditions were imposed in all directions. The long range electrostatic interactions have been calculated without any truncation, while a 9Å cutoff was applied to Lennard-Jones interactions. The non-bonded pair list was updated every 20 steps and all covalent bonds were constrained at their equilibrium distances by using SHAKE algorithm, which allowed us to use a 2 fs integration time. The structures were saved after every 100 steps, i.e. at every 0.2 ps interval, for the entire duration of the MD run.

Initial systems were energy minimized to an r.m.s gradient of 0.1 kcal/mol- Å. All the waters and surrounding counter ions were subjected to 20 ps dynamics at 100K, keeping DNA and coordinated ions fixed, followed by an energy minimization of the entire system. The quenched system was then heated slowly, from 0K to 300K, by coupling to a heat bath whose temperature was raised at the rate of 50K for every 2 ps of MD run. The system was equilibrated for another 88 ps and the dynamics run continued for a further 1 ns during which the structures were coupled

to a heat bath at 300K with a coupling constant of 0.1 ps. In order to know the stability of quadruplex structure at higher temperature and facilitate coordinated ion movement, both the systems temperature were raised upto 400K and simulations were continued for another 1 ns. Thus, total simulation time for both the AP-Na and AP-K structures are 2.1 ns. In all our analysis, terminal tetrad at the 5' end of the reference first strand (with a *syn* glycosidic conformation) is denoted as tetrad 1 and tetrad 7 is the terminal tetrad at the 3' end of the first strand. MD average structures in both the simulations are obtained from the coordinates saved between 100 to 1100 ps. All the structural parameters are calculated using the program NUPARM (63-64). The energies were calculated using ANAL module of AMBER 4.1 and the trajectories are plotted using MATLAB package.

Results and Discussion

Na^+ Ion Coordinated Antiparallel Structure is More Flexible Than the K^+ Ion Coordinated Structure

The root mean square (rms) deviation profiles during both the MD simulations are calculated with respect to the initial energy minimized model built structures and shown in Figure 2. It is seen that the Na^+ ion coordinated quadruplex reaches full

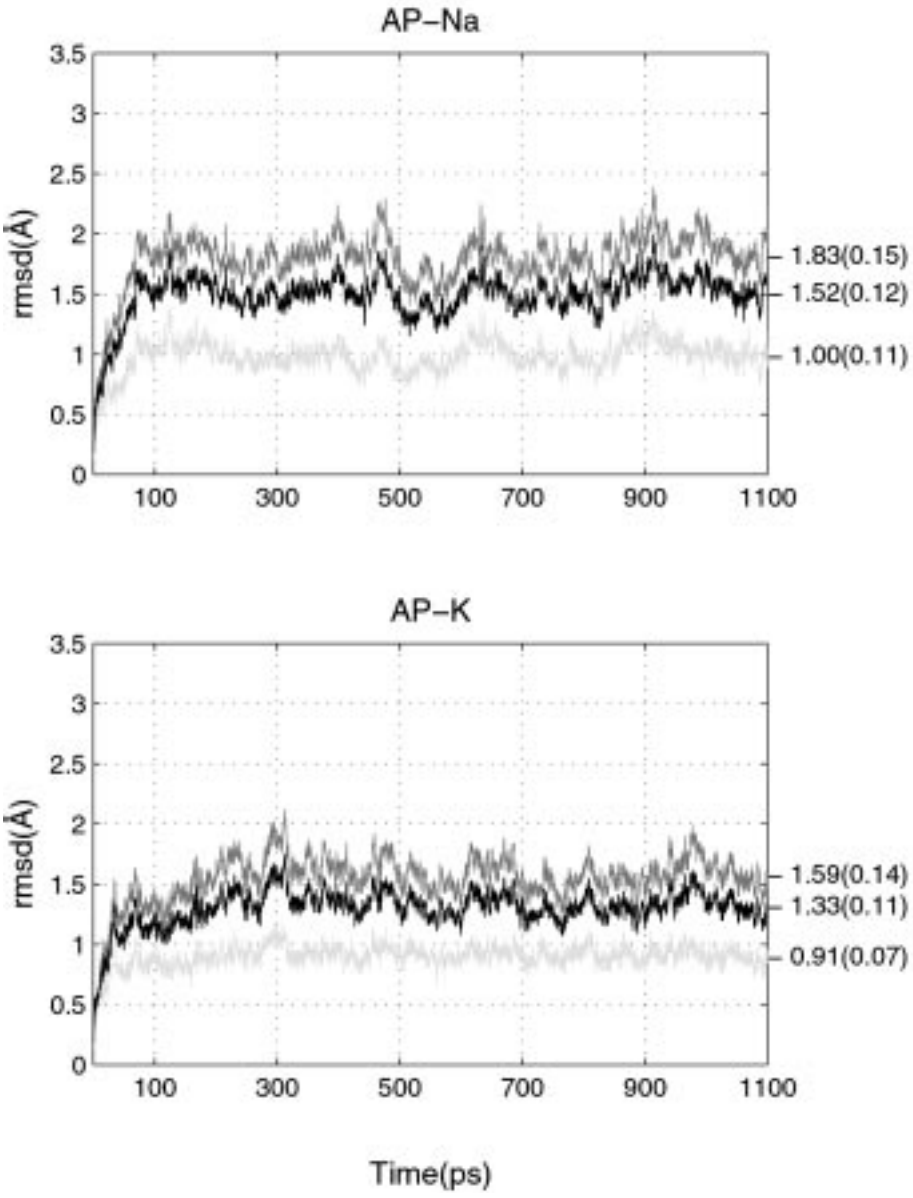

Figure 2: Root mean square (rms) deviation profiles, during the MD simulation of AP-Na and AP-K d(G_7) antiparallel quadruplexes, with respect to their respective initial energy minimized structures. The mean value of rmsd between 100 to 1100 ps interval is indicated on the right hand side of each plot while the standard deviation is given within parenthesis. The three plots, from top to bottom, correspond to the rmsd for the phosphodiester backbone with sugar, all the atoms and the guanine bases alone. In both the simulations rms deviations for base atoms are smallest while they are largest for sugar and backbone atoms.

equilibration within 100 ps. However, backbone in the K^+ ion coordinated structure requires 300 ps to equilibrate. The rms deviation of base atoms in both the simulations are ~0.8 Å less than the corresponding backbone atoms, indicating larger fluctuations in backbone atoms. Antiparallel quadruplex with coordinated K^+ ion has marginally lower mean rms deviation values (indicated on the right hand side of the Figure 2) than that of coordinated Na^+ ions structure. Thus, during the simulation, in comparison with AP-K structure, larger structural changes occur in Na^+ ion coordinated antiparallel structure. However, the overall structural features in both Na^+ and K^+ ion coordinated antiparallel structures are very similar. Stereo diagrams of both MD average quadruplex structures, obtained from the 100-1100 ps of dynamics are shown in Figure 3A-B along with the coordinated ions in their average positions. The middle four nucleotides (3rd, 4th, 5th and 6th) of Na^+ coordinated MD average structures are superimposed on corresponding K^+ ion coordinated MD average structure and shown in Figure 4A. It is observed that backbone, as well as base tetrads of these two structures are nicely overlapped with one another (rms deviation is 0.81Å), even though local tetrad geometry in the two structures differs significantly. This is apparent from Figure 4B, which shows the superimposition plot of 4th tetrad, in both the MD average antiparallel structures. It is clear that the orientation of guanine bases within a tetrad, and consequently the hydrogen bonding scheme are not identical in the two structures. This is discussed in detail in a later section. During the elevated temperature simulation (1.1 to 2.1 ns), both the quadruplex structures as well as ions showed considerably larger deviation from their respective energy minimized structures. However, the AP-Na structure retains its tetrameric form while in AP-K structure, the structure tends to fray at the 3′ terminal of strand 1. Interestingly, at the end of 1 ns dynamics at 400K, the rms deviation of middle four tetrads in AP-K structure with respect to the middle four tetrads in MD average AP-K structure obtained during 300K simulation, is consid-

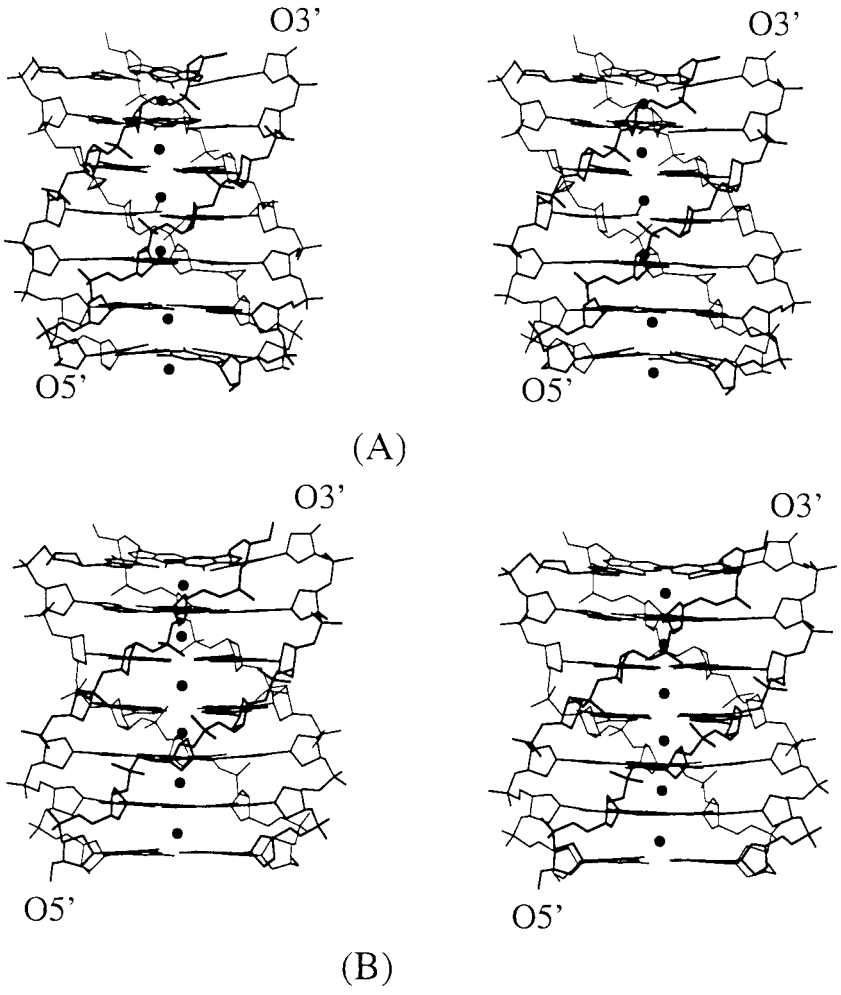

Figure 3: Stereo diagrams showing the MD average structure obtained from the 100-1100 ps of dynamics for **(A)** AP-Na quadruplex with coordinated Na^+ ions and **(B)** AP-K quadruplex with coordinated K^+ ions. Filled circles represent mean position of coordinated ions for both the structures. It is seen that one of the coordinated Na^+ ions in AP-Na has come out of the quadruplex core.

erably smaller (0.91Å) than that in AP-Na structure (1.58Å). This clearly indicates that even at the higher temperature, the G-tetrads with the K^+ coordinated ions are held together quite rigidly, while the quadruplex structures are maintained with both Na^+ and K^+ ions.

Hydrogen Bonding Patterns

G-tetrads in quadruplex structures are mainly stabilized by cyclic Hoogsteen type (N1-H1···O6 and N2-H2···N7) hydrogen bonds. Average inter atomic distances between potential hydrogen bond forming groups within a G-tetrad and distances between different O6 atoms in both the MD average AP-Na and AP-K structures obtained during the 100-1100 ps dynamics run, are listed in Table I. During the simulation, standard Hoogsteen type N1-H1···O6 and N2-H2···N7 hydrogen bonds (acceptor to hydrogen distance is < 2.6Å) in all G-tetrads are retained for AP-Na structure. However, due to the strong attractive force between coordinated Na^+ ion and O6 atoms, guanine bases in some G-tetrads undergo in-plane rotational motion. Because of this rotational motion, N1-H1···O6 hydrogen bonds are elongated, whereas N1 atom of guanine base comes closer to N7 atom of neighbouring guanine base and forms a N1-H1···N7 hydrogen bond. Thus, in these cases, tetrads are stabilized by three centered hydrogen bonds. As observed in Table IA, tetrads 1, 4, 5, 6, and 7 in AP-Na structure, are stabilized by three centered hydrogen bonds and tetrads 2 and 3 are stabilized by standard Hoogsteen type hydrogen bonds. In the case of AP-K structure, the larger in-plane rotational motion of guanine bases in the middle G-tetrad (4^{th}) leads to a G-tetrad stabilized only by cyclic N1-H1···N7 hydrogen bonds while tetrad 5 is stabilized by three centered hydrogen bonds and normal Hoogsteen type hydrogen bonds are retained in all other tetrads (Table IB).

The distances between O6 atoms on adjacent and diagonal guanines in a G-tetrad also indicate in-plane base rotation for some of the G-tetrads (listed in Table I). In both the AP-Na and AP-K structures, the adjacent and diagonal O6—O6 distances, for the G-tetrads with three centered hydrogen bonds, are considerably smaller than the corresponding distances in G-tetrads with normal Hoogsteen type hydrogen bonds. In the presence of coordinated cations, in-plane base rotation within a G-tetrad brings O6 atoms close to one another. Due to the presence of larger K^+ ion, these O6—O6 distances in K^+ ion coordinated structure are ~0.5 Å longer than the distances in the Na^+ ion coordinated antiparallel structure. Interestingly, average values of inter atomic distances between hydrogen bond forming groups and average distances between different O6 atoms over the seven tetrads in AP-K structure (listed in Table IB) are close to the average values in the $(G_4T_4G_4)_2$ crystal structure (20) with potassium salt, though only one coordinated ions has been identified in the central cavity.

Interaction Energy Within a G-tetrad and Stacking Energy Between Successive G-Tetrads

During the MD simulation, base interaction energies (van der Waals and electrostatic) were calculated within a G-tetrad, and the average interaction energies for each of the 7 G-tetrads over 100 to 1100 ps simulation are listed in Table II for both AP-Na and AP-K structures. It is noticed that the base-base interaction energy, within a G-tetrad largely depends on hydrogen bonding pattern and electrostatic interaction between different polar atoms. G-tetrads with larger separation between in-plane O6 atoms and with standard Hoogsteen type (cyclic N1-H1··O6 and N2-H2··N7) hydrogen bonds have more favourable base interaction energy. Only second and third tetrads in AP-Na structure are stabilized by normal Hoogsteen type hydrogen bonds and adjacent as well as, diagonal O6—O6 distances in these tetrads are larger than the other G-tetrads. Therefore, base interaction energies in these two tetrads are more favourable than other G-tetrads. Due to the rotational motion of guanine bases, other G-tetrads, in AP-Na structure are stabilized by three

centered hydrogen bonds and O6 atoms come closer together, leading to unfavourable electrostatic interaction energy and hence less favourable base interaction energy. Similarly, in case of AP-K structure, the G-tetrads at both the terminals are stabilized by standard Hoogsteen type hydrogen bonds (Table IB) and thus have more favourable base interaction energies. Rotational motion of guanine bases within a G-tetrad is more pronounced in the middle part of AP-K quadruplex structure and maximum for the 4th G-tetrad, giving rise to positive electrostatic interaction energy for 4th tetrad and unfavourable base interaction energy. However, the interaction energy between the coordinated ion and adjacent single G-tetrad has large negative value (this contribution being ~ -111.5 kcal/mol for AP-Na and ~ -96.9 kcal/mol for AP-K.). Hence, irrespective of tetrad orientation, the total energy for each tetrad, alongwith one associated ion is highly favourable for both the AP-Na and AP-K structures.

Due to close clustering of negatively charged O6 atoms of guanines, electrostatic energy component of the base stacking energy between successive G-tetrads is repulsive and total base stacking energies for both the structures are close to zero (~ -2.1 and ~ -0.6 kcal/mol for AP-Na and AP-K respectively). However, in both the structures, van der Waals component of base stacking energy is favourable and close to ~ -43.0 kcal/mol. Stacking diagrams of the 5th tetrad over the 4th one in AP-Na and AP-K structures are shown in Figure 5A and 5B. It is observed that in both the structures, six-member ring of guanine base in upper tetrad is completely stacked over the six-member ring of bottom guanine. In both Na^+ and K^+ ion coordinated structure, inclusion of the energy contribution, due to coordinated ions pro-

Table I

Average values of inter atomic distances (in Å) between potential hydrogen bond forming groups within the G-tetrads in the MD average structures (100-1100 ps) are shown **(A)** AP-Na **(B)** AP-K along with the average values in the crystal structure (20) with potassium salt. The distances between O6 atoms on adjacent and diagonal guanines in the tetrad, as well as between opposite corners of twisted cube formed by O6 atoms are also listed. Standard deviations are shown in parenthesis. Average distances over all seven G-tetrads are shown in the last row of each table, along with their standard deviations.

(A) AP-Na

	N1--O6/H1--O6		N2--N7/H2--N7		N1--N7/H1--N7		O6-O6[a]	O6-O6[b]	O6-O6[c]
Crystal	3.18	2.36	2.97	2.10	3.48	2.84	3.07	4.16	5.45
Structure	(0.28)	(0.39)	(0.28)	(0.32)	(0.53)	(0.64)	(0.49)	(1.0)	(0.86)
Tet-1	2.86	2.07	2.65	1.76	3.08	2.36	2.67	3.77	4.94
Tet-2	2.74	1.88	2.69	1.78	3.39	2.72	2.86	4.04	4.97
Tet-3	2.73	1.88	2.67	1.77	3.37	2.70	2.85	4.03	5.01
Tet-4	2.86	2.08	2.67	1.78	3.10	2.36	2.67	3.77	4.77
Tet-5	2.95	2.19	2.73	1.85	3.06	2.30	2.67	3.76	4.85
Tet-6	3.00	2.24	2.76	1.88	3.05	2.27	2.68	3.78	4.83
Tet-7	2.80	1.97	2.64	1.74	3.21	2.51	2.77	3.92	
Average	2.85	2.05	2.69	1.79	3.18	2.46	2.74	3.87	4.90
Std. dev.	(0.11)	(0.15)	(0.05)	(0.06)	(0.15)	(0.19)	(0.09)	(0.20)	(0.34)

(B) AP-K

	N1--O6/H1--O6		N2--N7/H2--N7		N1--N7/H1--N7		O6-O6[a]	O6-O6[b]	O6-O6[c]
Tet-1	2.86	1.90	2.89	1.93	3.87	3.21	3.27	4.62	5.43
Tet-2	3.05	2.18	2.90	1.94	3.45	2.67	2.96	4.18	5.12
Tet-3	3.01	2.15	2.88	1.92	3.42	2.65	2.92	4.12	5.22
Tet-4	4.28	3.70	3.81	3.17	2.95	1.98	2.97	4.20	5.41
Tet-5	3.10	2.26	2.93	1.97	3.39	2.59	2.93	4.13	5.31
Tet-6	3.09	2.24	2.92	1.96	3.42	2.63	2.95	4.16	5.14
Tet-7	2.87	1.92	2.86	1.90	3.84	3.17	3.28	4.64	
Average	3.18	2.34	3.03	2.11	3.48	2.70	3.04	4.29	5.27
Std. dev.	(0.46)	(0.57)	(0.32)	(0.43)	(0.29)	(0.38)	(0.15)	(0.22)	(0.14)

[a]Distance between adjacent O6 atoms in a G-tetrad

[b]Distance between diagonally opposite O6 atoms within a G-tetrad

[c]Distance between diagonally opposite O6 atoms in the twisted cube formed by O6 atoms in two neighbouring G-tetrads

Table II

Interaction energies between the bases within a G-tetrad in Na^+ and K^+ ion coordinated antiparallel structures are shown. Total interaction energy is divided into van der Waals and electrostatic components. Energies (in kcal/mol) are averaged over the 1000 structures obtained during 100-1100 ps of dynamics. Standard deviations are listed within parentheses.

	AP-Na			AP-K		
	vdW	e.s.	Total	vdW	e.s.	Total
Tet-1	-4.4	-25.7	-30.1	-3.1	-52.8	-55.9
	(2.4)	(7.3)	(6.5)	(2.1)	(6.3)	(4.9)
Tet-2	-2.6	-41.8	-44.4	-5.4	-31.4	-36.8
	(2.9)	(8.9)	(7.5)	(2.5)	(8.0)	(6.6)
Tet-3	-2.9	-43.0	-45.9	-4.3	-32.2	-36.5
	(2.7)	(5.7)	(4.4)	(2.5)	(6.5)	(5.5)
Tet-4	-7.6	-6.3	-13.9	-9.6	18.1	8.5
	(2.0)	(6.7)	(5.9)	(1.2)	(3.5)	(3.6)
Tet-5	-4.1	-21.2	-25.3	-5.8	-26.5	-32.3
	(2.2)	(8.7)	(8.0)	(2.3)	(7.6)	(6.3)
Tet-6	-5.2	-19.7	-24.9	-5.7	-28.4	-34.1
	(2.5)	(9.0)	(8.2)	(2.2)	(9.7)	(8.4)
Tet-7	-3.6	-35.1	-38.7	-3.0	-51.3	-54.3
	(2.9)	(8.7)	(7.5)	(2.5)	(7.9)	(6.7)
Mean	-4.4	-27.5	-31.9	-5.3	-29.2	-34.5
Std. dev.	(3.0)	(14.6)	(12.8)	(3.1)	(22.9)	(20.6)

duces favourable stacking energy. Average stacking energy between 2^{nd} and 3^{rd}, 3^{rd} and 4^{th}, 4^{th} and 5^{th}, 5^{th} and 6^{th} and between 6^{th} and 7^{th} tetrads in AP-Na and AP-K structures are calculated during 100 to 1100 ps dynamics and listed in Table III. In this calculation, G-tetrad and coordinated ion on its 5′ side are considered as one group and the neighbouring G-tetrad alongwith the coordinated ion on its 5′ side is considered as the second group. Total stacking energy consists of base tetrad stacking energy, the interaction between successive coordinated ions, as well as interaction energies between the coordinated ion and the neighbouring G-tetrad. It is observed that the electrostatic components of interaction energies, related with coordinated ions, make the largest contribution. It is also found that the coordinated Na^+ ions in AP-Na structure can move along the quadruplex axis and affect the stacking energy values. Because of coordinated Na^+ ions movement, distance between successive coordinated ions increases during the simulation and hence, the repulsion between the two positively charged ions decreases. For this reason, the stacking energy between tetrad 3 and tetrad 4 in AP-Na structure is most favourable. However, in case of tetrads 2 and 3 as well as tetrads 6 and 7, due to

Table III

Stacking energy values in Na^+ and K^+ ion coordinated antiparallel quadruplex structures are listed. Stacking energies are averaged over the 1000 structures obtained during 100-1100 ps of molecular dynamics simulation. Stacking energy between 2^{nd} - 3^{rd}, 3^{rd} - 4^{th}, 4^{th} - 5^{th}, 5^{th} - 6^{th} and 6^{th} - 7^{th} tetrads are shown. G-tetrad and coordinated ions on its 5′ side is considered as one group and neighbouring G-tetrads alongwith the coordinated ion on its 5′ side are considered as second group. Total stacking energy is divided into van der Waals and electrostatic components. All energy values are in kcal/mol. Standard deviation values are shown in parentheses.

	AP-Na			AP-K		
	vdW	e.s.	Total	vdW	e.s.	Total
Tet23	-34.9	-9.8	-44.7	-34.6	-3.3	-37.9
	(2.5)	(6.9)	(6.4)	(2.2)	(6.6)	(6.4)
Tet34	-34.8	-42.4	-77.2	-35.8	-3.8	-39.6
	(3.0)	(12.1)	(11.0)	(1.8)	(5.6)	(5.0)
Tet45	-37.3	-21.4	-58.7	-33.8	-13.7	-47.5
	(2.2)	(13.5)	(12.0)	(2.1)	(5.5)	(5.1)
Tet56	-39.5	-15.4	-54.9	-33.8	-10.4	-44.2
	(1.7)	(8.8)	(8.0)	(2.3)	(5.9)	(5.5)
Tet67	-40.4	-0.8	-41.2	-37.5	-0.4	-37.9
	(1.6)	(13.9)	(12.0)	(2.3)	(10.6)	(10.0)

the outward movement of coordinated ions, distance between coordinated ion and G-tetrad increases and electrostatic energy component as well as stacking energy becomes less favourable. In case of AP-K structure, no noticeable movement is observed for the coordinated K^+ ions, through the quadruplex channel. Therefore, the stacking energy values between all successive tetrads are much more uniform. However, stacking energy between tetrad 4 and tetrad 5 is most favourable due to more favourable interaction energy between guanine bases in 4th tetrad (which is stabilized only by cyclic N1-H1···N7 hydrogen bond) and coordinated K^+ ion.

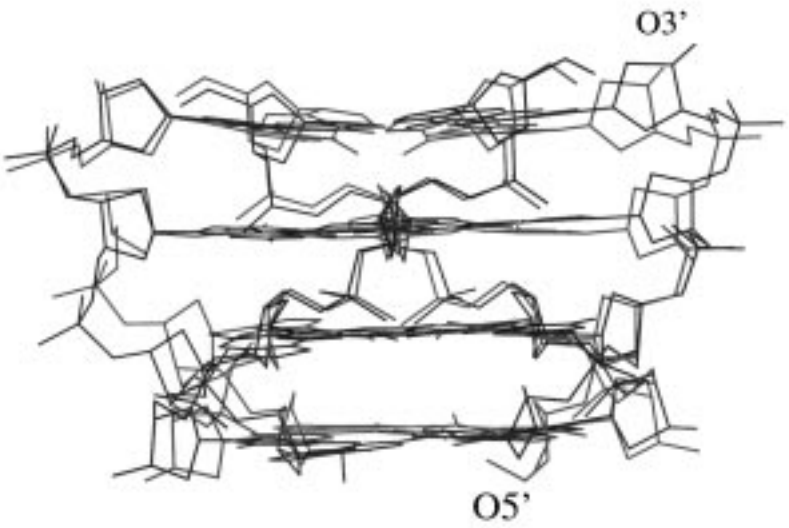

(A)

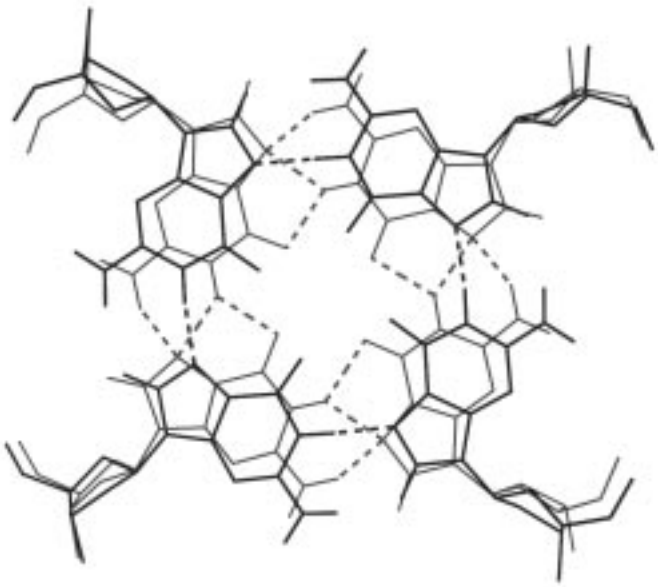

(B)

Figure 4: (A) Middle four nucleotides (3rd, 4th, 5th and 6th) in MD average AP-K (blue lines) is superimposed on the Na^+ ion coordinated AP-Na structure (red lines). The rms deviation between all atoms in the AP-K structure with respect to the AP-Na structure is 0.81Å while it is 0.70Å for the G-tetrads. **(B)** Middle G-tetrad (4th tetrad) of MD average AP-K structure (blue lines) is superimposed on corresponding tetrad in the AP-Na structure (red lines). Hydrogen bonding schemes in both the tetrads are shown by dotted lines.

In order to examine the movement of coordinated ions, ion-O6 distance trajectories have been plotted for both the simulations and are shown in Figure 6. During the molecular dynamics simulations, the behaviour of coordinated Na^+ ions is quite

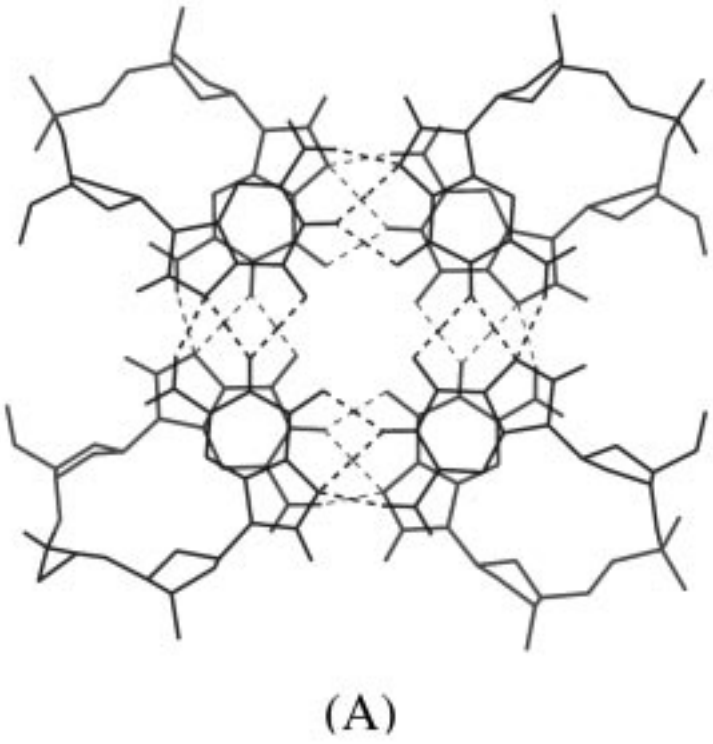

Figure 5: Stacking and hydrogen bonding patterns in the 4th and 5th tetrads in MD average structures for **(A)** AP-Na and **(B)** AP-K. Hydrogen bonds with hydrogen to acceptor atom distance < 2.6 Å, are indicated by dotted lines. The upper tetrad (i.e. 5th tetrad) is drawn in blue lines while the lower tetrad is in red lines. The step corresponds to an *anti-syn* step.

different from that of K^+ ions. Coordinated Na^+ ions move along the quadruplex axis as indicated by large fluctuation in the Na^+-O6 distances (Figure 6) as well as distance between adjacent Na^+ ions (data not shown) whereas the K^+ ions are almost stationary throughout the whole simulation. Coordinated Na^+ ion at the 5′ terminal of strand 1 moves out from the quadruplex core within the equilibration period but remains coordinated with O6 atoms in the outermost tetrad 1, as it is observed that the distances between first Na^+ ion and O6 atoms of tetrad 2 are very large (Figure 6). Simultaneously the second coordinated ion between tetrads 2 and 3 moves to occupy the vacant first coordination site, leaving the second coordination site vacant. The movements of these two Na^+ ions along the quadruplex axis are illustrated in Figures 7A and 7B. Snap shots of the first three tetrads, at different point of time during the simulation, are superimposed and the outward movement of the ion that is initially located between the first and second tetrads is shown in Figure 7A, whereas the movement of the ion, coordinated between the second

Figure 6: Trajectories showing the distances between the coordinated ions and neighbouring O6 atoms in the AP-Na and AP-K structures. All 6 coordinated ions and their distances from neighbouring O6 atoms in the first and second strands are shown. Time (in ps) is along x-axis and ion—O6 distances in Å are along y-axis. Figure 6 continued on the following page.

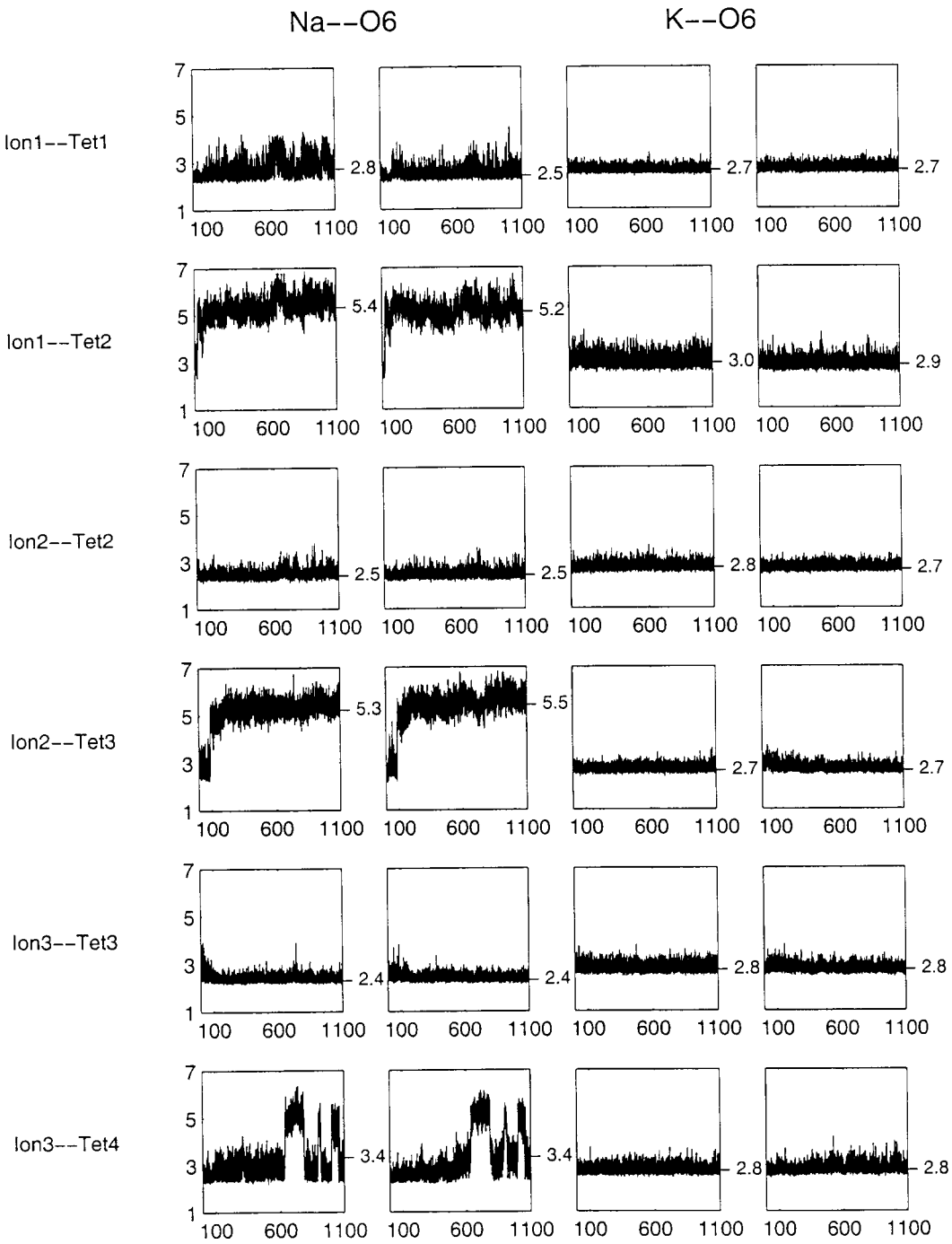

and third tetrads is shown in Figure 7B. The third coordinated ion also moves along the central axis and partially occupies the vacant second coordination site between the second and third tetrads (mainly between 600 to 700 ps). Thus, both second and third coordination sites remain partially unoccupied, as seen in the stereo diagram of the average structure (Figure 3A). Even though the starting 7-mer antiparallel quadruplex structure is perfectly symmetric with respect to a dyad axis located in the plane of the tetrad-4, due to the relative movement of three coordinated Na^+ ions at the 5′-side of the AP-Na structure, the G-tetrads geometry, intra tetrad base interaction energy and stacking energy (which include contribution due to the associated ions) are not equivalent for the symmetry equivalent positions (as observed in Tables IA, II and III). However, the K^+ ion coordinated AP-K structure is much more symmetric due to these larger ions remaining close to their symmetrically related initial positions. Our earlier MD simulations on parallel quadruplex structures have also demonstrated that the 1st and 7th, 2nd and 6th, 3rd and 5th base tetrads

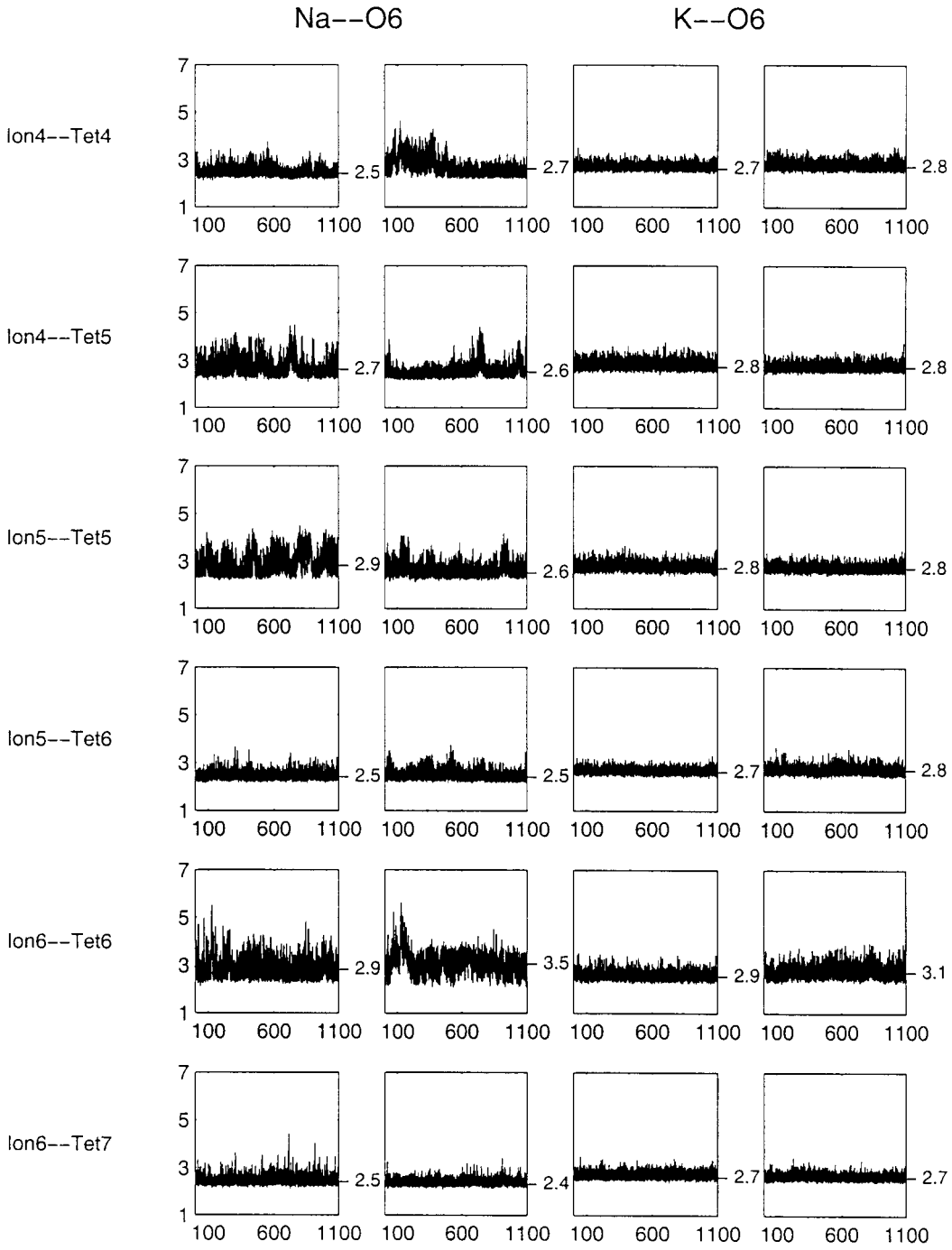

Figure 6 continued.

in the parallel quadruplex structures (52) are structurally and energetically more or less equivalent, even though the aforesaid dyad axis is absent in the parallel quadruplex structures, suggesting that the effect of solvent and coordinated ions are more dominant in the quadruplex structure. In our molecular dynamics simulation at room temperature, the larger K^+ ions are not allowed even temporary in-plane coordination within a G-tetrad plane and the K^+ ions remain within their respective cavities. The movement of coordinated Na^+ ions is reflected in their interaction energy with other atoms in the cell as shown in the plots of Figure 8. It is observed that the coordinated Na^+ ion at the 5′ end of the AP-Na structure, which moves out from the quadruplex core and the ion between tetrads 2 and 3 as well as the ion between tetrads 3 and 4 which show some mobility have less favourable interaction energy as compared to the coordinated ions at the 3′ end of the quadruplex. In both AP-Na and AP-K structures, due to larger ion-ion repulsive energy, coordinated ions located at the middle of quadruplex structures have less favourable interaction energy as compared to the coordinated ions at both the ends. In case of AP-Na structure, average interaction energy of solvent ions (representative example shown in last row of Figure 8) is comparable with the average interaction energy of coordinated ions. However groove bound ions, which interact with both DNA and solvent, have marginally better interaction energy for both AP-Na and AP-K structures (as seen from the seventh row in Figure 8). In case of AP-Na quadruplex, average interaction energy of coordinated Na^+ ions are more favourable than the interaction energy of coordinated K^+ ions in AP-K structure. During the 1ns elevated temperature simulation, the coordinated Na^+ ion, which had already come out from the quadruplex core, moves further away from DNA and equilibrates with the solvent. However, the other five coordinated Na^+ ions remain inside the quadruplex channel. In the case of K^+ ion coordinated structure, the 3′ terminal coordinated K^+ ion moves out from the DNA core by disrupting the tetrad geometry at the 3′ terminus, during the elevated temperature simulation (at 400K) and equilibrates with the solvent molecules. This is clearly observed in Figures 9A and 9B, which show stereo diagrams of snap shots at the end of elevated temperature simulations and

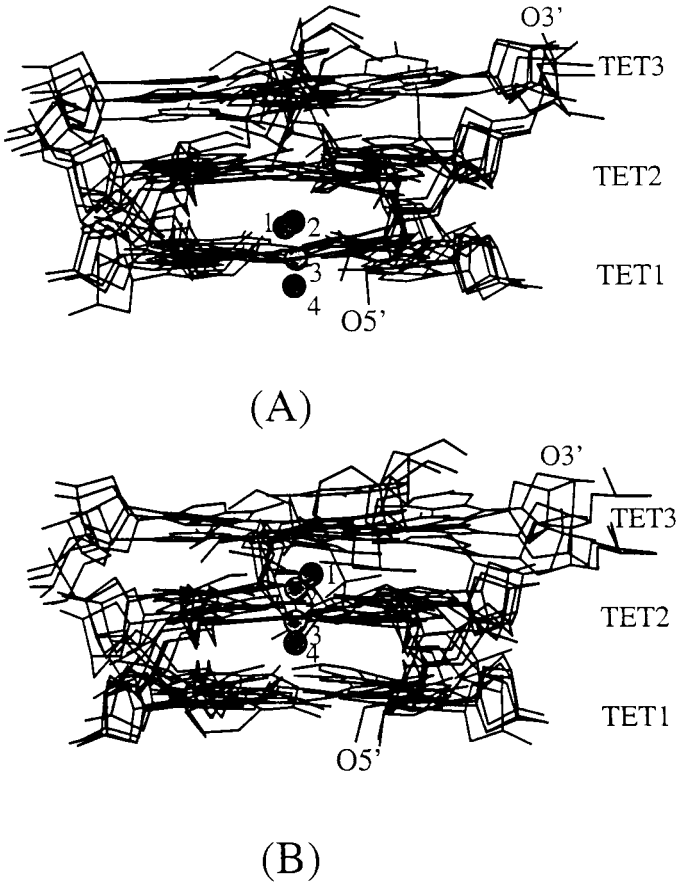

Figure 7: Superimposed snap shots of three terminal G-tetrads in AP-Na structures, at four different time points during the MD simulations, showing movement of two coordinated ions. In each case, as the simulation progresses, the coordinated ion moves from position 1 to 4, through positions 2 and 3 **(A)** Movement of the 1st ion from a location between tetrads 1 and 2 to a position outside the quadruplex stem and **(B)** Movement of 2nd ion between tetrads 2 and 3 to a location between tetrads 1 and 2. The sampling time for (A) is 0-50 ps whereas it is 90-150 ps for (B). The 5′ and 3′ ends of ascending strand 1 in the antiparallel Greek key type quadruplex structure are indicated by O5' and O3′.

subsequent quenching to 300K, for both the quadruplex structures.

During the simulation, solvated Na^+ counter ions in both the systems traverse through considerable distance and bind in the two smaller grooves of these antiparallel Greek key type quadruplexes. For both the simulations it is observed that on an average, 8 Na^+ counter ions are within 3.5 Å of DNA and most of them are within the two smaller grooves (with smaller groove width ~7.0 Å while larger groove width is ~13.0 Å). Na^+ counter ions, in both the simulations tightly fit into the smaller grooves of antiparallel quadruplex structures and are coordinated with oxygen atoms of the DNA backbone. In both the AP-Na and AP-K structures, the positions of solvent ions, which stay within the 3.5 Å of DNA atom for more than 50 % of dynamics time, are shown in Figures 10A and 10B. In case of Na^+ ion coordinated AP-Na structure, three Na^+ counter ions bind into the smaller groove between the strand 1 and strand 2 (counter ions are localized more than 50% of total dynamics time). Similarly, four counter ions are bound to the other small groove between strand 3 and 4 (more than

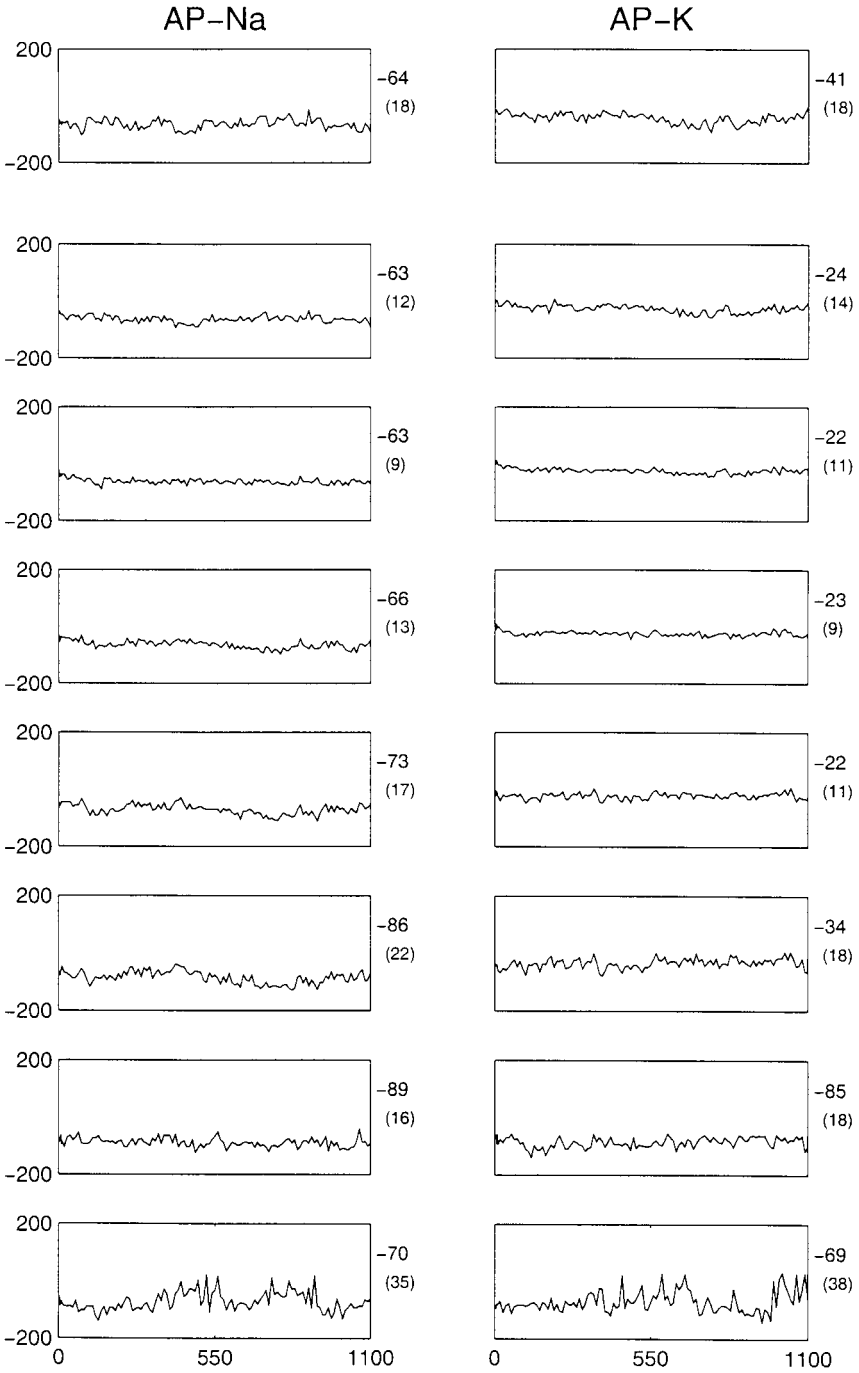

Figure 8: Trajectories showing the interaction energy between individual ion to all other atoms in the simulated cell during the MD simulations. Time (in ps) is along x-axis and interaction energy (in kcal/mol) is along y-axis. Average interaction energy values alongwith their standard deviations (within parenthesis) in the period between 100 to 1100 ps, are indicated at the right hand side of each plot. In the both AP-Na and AP-K structures, the first six rows represent interaction energy of coordinated Na^+ or K^+ ions with all other atoms, with the coordinated ion at the 5′ end being at the top, while the 7^{th} and 8^{th} rows show interaction energy of a representative groove bound (within 3.5 Å of DNA atom) and free solvent Na^+ ion respectively.

50% of dynamics time). Solvent counter ions, in the K^+ ion coordinated antiparallel structure are also bound only to the smaller grooves of the quadruplex structure. Two ions are bound deep inside the small groove, between strand 1 and strand 2, while another two ions are seen inside the other small groove formed between strands 3 and 4. Interestingly, during the elevated temperature dynamics, a few of the solvent counter ions in both the simulations still occupy the positions within the smaller grooves and stay close to the positions shown in Figure 10A and 10B. Representative interaction energies for smaller grooves bound ion and free solvent ions are shown in the last two rows of Figure 8 which indicates that the mean interaction energy of groove bound ions is about 18 kcal/mol more favourable than the energy for the unbound ions. Thus, the two smaller grooves, in both the Na^+ and K^+ ion coordinated antiparallel structures, are more favourable binding sites for Na^+ counter ions, as

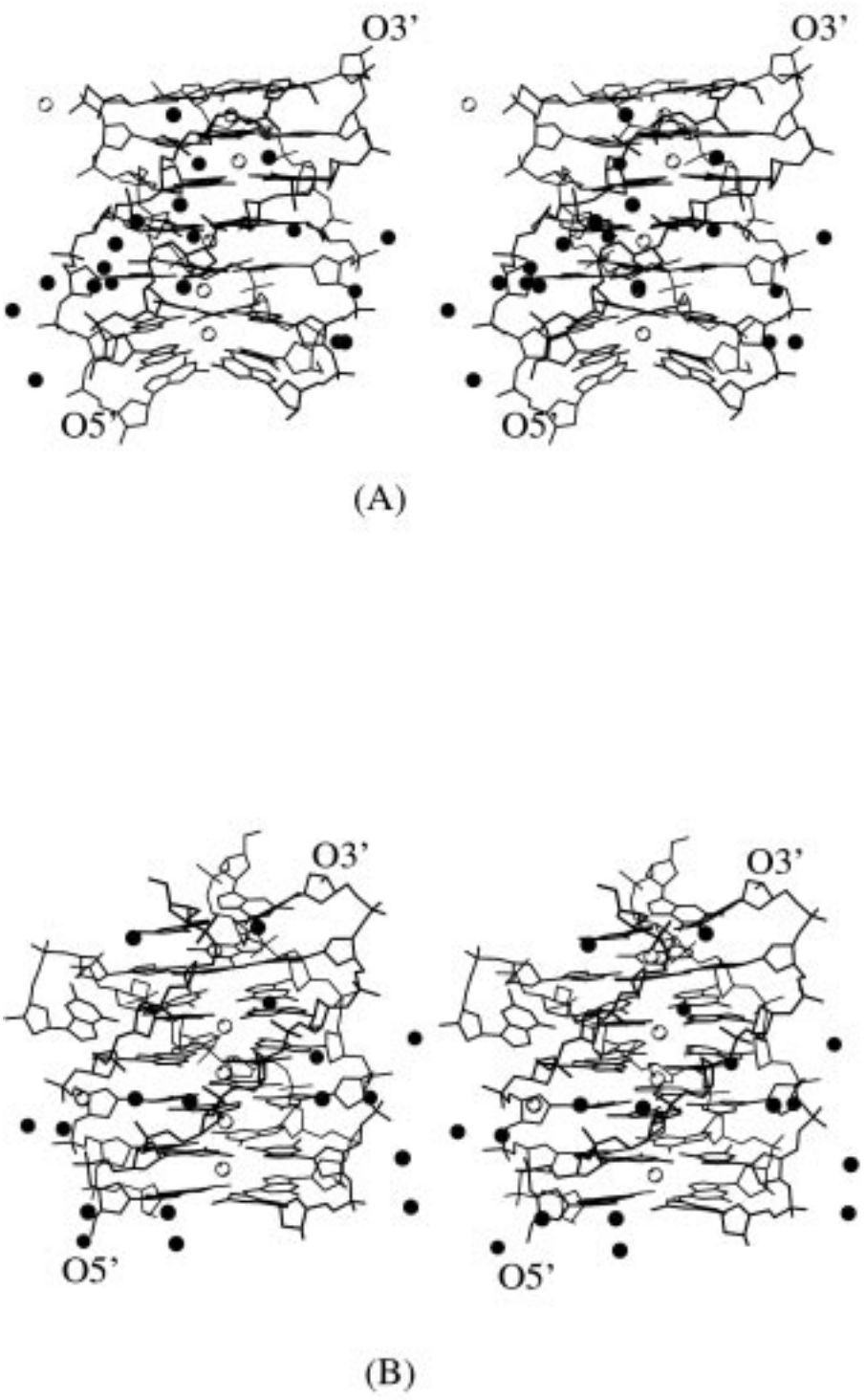

Figure 9: Stereo diagram of the **(A)** AP-Na and **(B)** AP-K quadruplex structures at the end of 1 ns of MD at 400K and subsequent quenching to 300K. The solvent counter ions (within 5.0 Å cut off distance from quadruplex) are shown in red (filled circles) and initial coordinated ions are shown as green circles. It is seen that the Na^+ ions move out of the central cavity without disruption of the quadruplex, while the forced movement of K^+ ions causes the AP-K structure to be frayed at one end.

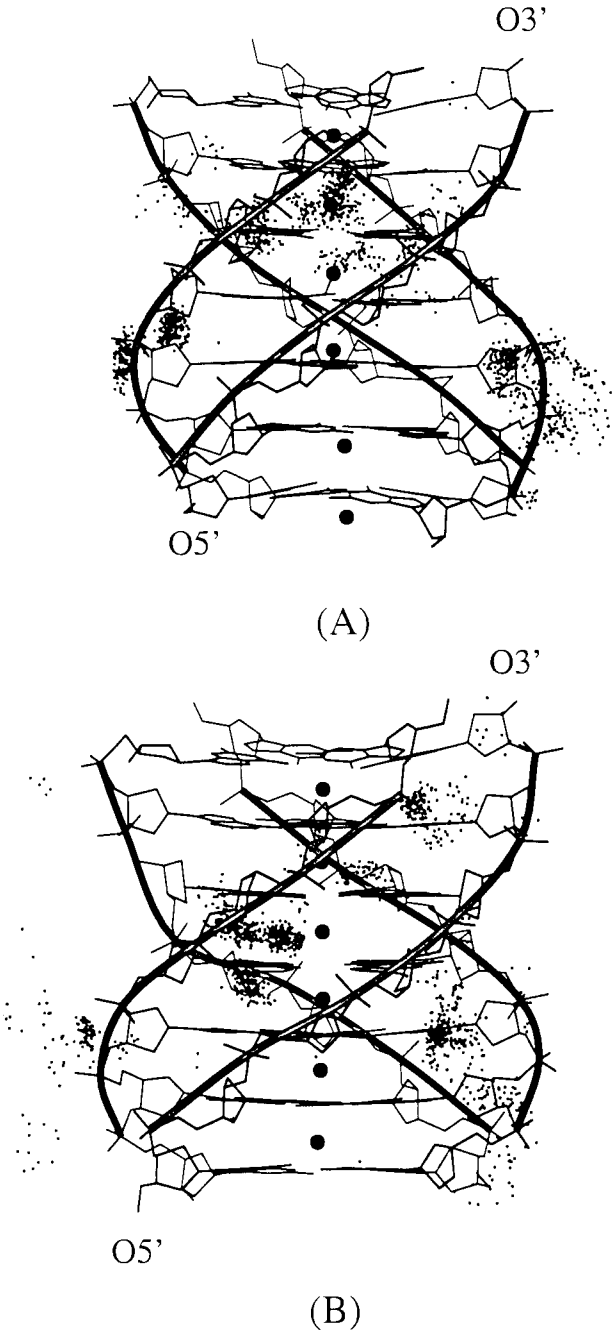

Figure 10: MD average quadruplex structure along with the positions of counter ions within 3.5 Å of DNA atoms in (**A**) AP-Na and (**B**) AP-K quadruplexes. Black dots represent position of Na^+ counter ions. Only the counter ions, which stay within 3.5 Å of DNA atoms for more than 50% of dynamics time (between 100 to 1100 ps) are considered. The mean positions of the coordinated ions are shown as filled circles while a ribbon is drawn through the phosphodiester backbone.

compared to the two larger grooves.

Hydration Pattern

Several experimental and theoretical studies have already showed the existence of spine of water molecules in the grooves of double stranded DNA structure (60,65-67). The water molecules inside the groove tend to lie either in-plane with the Watson-Crick base pairs, or between two base pair planes and form hydrogen bond with exposed polar base atoms. Systematic analysis of hydration sites (68) in DNA crystal structures has revealed that in A-DNA major groove, guanine has two main hydration sites with solvent molecules interacting with O6 and N7 atoms, while the minor groove has a single low density hydration site that interacts with both N3 and N2 atoms of guanines whereas in B-DNA N2 atoms of guanine are completely unhydrated. Similar analysis on Z-DNA crystal structure showed that positions near guanine N2 atoms are the most favourable hydration site. Similarly, crystal structure of the parallel G-quadruplex (21) showed that quadruplex grooves are favourable binding sites for water molecules, which form hydrogen bonds with both

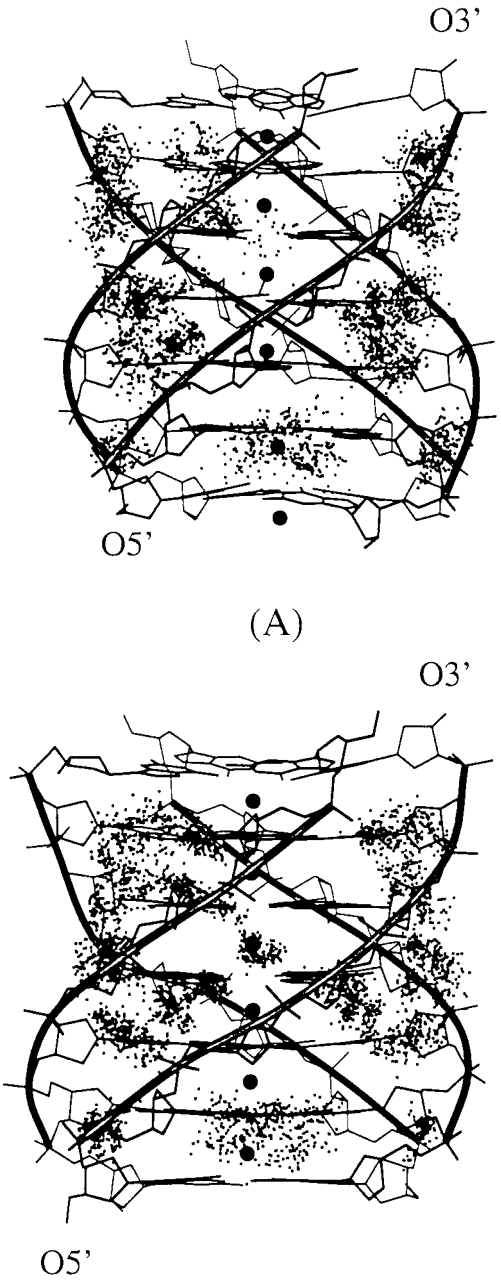

Figure 11: MD average structure is shown along with the hydration pattern around the middle five base tetrads in (**A**) AP-Na and (**B**) AP-K quadruplexes. Black dots represent position of oxygen atoms of water molecules, which stay within 3Å of guanine base atoms for more than 50% of dynamics time (between 100 to 1100 ps). The mean positions of the coordinated ions are shown as filled circles and phosphodiester backbone is outlined by a ribbon.

2-amino groups and N3 atoms. During the quadruplex simulation, distinct hydration patterns are observed for both the antiparallel structures. A ribbon of hydrogen bonded water molecules are observed within the two larger grooves in both the Na^+ and K^+ ion coordinated antiparallel quadruplex structures. These water molecules are close (within 3 Å) to the exposed 2-amino groups and N3 atoms and form hydrogen bonds. However, due to close proximity of sugar moiety, N3 atoms in guanine bases are partially shielded from water molecules. Consequently, N2 atoms emerged as more favorable binding sites for water molecules, as observed earlier in crystal structure of Z-DNA and parallel quadruplexes (21). In case of the two smaller grooves in both the antiparallel structures, due to the presence of counter ions, a few of the N2 and N3 atoms are protected from hydration. Hydration pattern around the base atoms of middle 5 tetrads (within 3 Å of any base atoms) in both the structures are shown in Figures 11A and 11B. In the case of Na^+ ion coordinated structure, two counter ions in this groove occur near tetrad 2 and tetrad 3, thus partially blocking the exposed amino group and N3 atom of guanine 13 (in tetrad 2), while the amino group and N3 atom of guanine 5 (in tetrad 5) remain completely unhydrated due to

presence of another counter ion near these atoms (as seen in Figure 11A). Similarly, in case of K^+ ion coordinated structure, due to presence of coordinated ion in the smaller groove between strand 1 and strand 2, amino groups and N3 atoms of guanine 3 (tetrad3), guanine 5 (tetrad 5) and guanine 9 (tetrad 6) are not hydrated. All other amino groups and N3 atoms in guanine bases remain hydrated during the entire MD simulation. Therefore, amino groups and N3 atoms of guanine bases are favourable binding sites for water molecules. However, due to groove binding counter ions, a few of the exposed amino groups, as well as N3 atoms of guanine bases, are inaccessible to water molecules.

Using the solvent accessible surface (SAS) area program of Connolly (69,70) with a probe radius of 1.4 Å and atomic solvation parameters (ASP) of Eisenberg and MacLachlan (71), we have quantitatively analyzed the free energy of hydration (ΔG_H) of guanine nucleotides. The free energy of hydration values have been calculated for both the MD average structures, using the procedure described by Kagawa *et. al* (72,73) ($\Delta G_H = \sum ASP_i \times SAS_i$ for each atom type 'i'). The ΔG_H values for the quadruplex fragment consisting of the middle five G-tetrads show that the hydration free energy of MD average AP-Na structure (-90.7 kcal/mol) is less favourable than the MD average AP-K structure (-102.8 kcal/mol). However, the hydration free energies of antiparallel structures (for both AP-Na and AP-K) are less favourable than the hydration free energy of corresponding MD average parallel quadruplex (52) structure with six coordinated ions (-109.0 kcal/mol and -108.9 kcal/mol for Na^+ and K^+ ions coordinated MD average parallel structures).

Backbone Torsion Angles and Structural Parameters

The backbone torsion angles, glycosidic torsion angles (χ) and pseudorotation phase angles (P) for both the structures are calculated during the simulations. It is observed that all backbone torsion angles in middle three nucleotides of first and second strands are well behaved during the both simulations and fluctuate within canonical B-DNA region i.e. α, β, γ, ε and ζ torsion angles are in *gauche*$^-$(*g*$^-$), *trans*(*t*), *gauche*$^+$(*g*$^+$), *trans*(*t*) and *gauche*$^-$(*g*$^-$) region respectively. The glycosidic torsion angles along a chain are alternating *syn-anti* and remain close to their respective region but pseudorotation phase angles fluctuate between O4′-*endo* and C2′-*endo* region. A few torsion angles in both the structures move to non-canonical region during the simulation. For example in the 3rd strand of AP-Na structure, ε values for all anti residues oscillate between *t* to *g*$^-$ region while a correlated transition in ζ from *g*$^-$ to *t* is observed only for the *anti* residue in fourth nucleotide. The α torsion angles of some nucleotides of both the structures undergo a transition from *g*$^-$ to *g*$^+$ region and β values oscillate between *t* to *g*$^-$ and *g*$^+$ regions, which is also observed in our earlier model building studies (22). A few of the γ torsion angles in both the structures also move from *g*$^+$ to *t* and *g*$^-$ region. As already discussed, some counter ions are bound to the two smaller grooves of antiparallel quadruplex structures and interact with oxygen atoms of phosphate groups. These interactions apparently facilitate the transition of backbone torsion angles. It is also observed that during the MD simulation, K^+ ion coordinated antiparallel quadruplex has less fluctuation in backbone torsion angles (data not shown) than the Na^+ ion coordinated structure, indicating that the AP-K structure is less flexible than the AP-Na structure.

The intra and inter basepair parameters have been calculated for MD average antiparallel quadruplex structures, taking the four strands pairwise and average values over the six steps are listed in Table IV. It is noticed that for both the structures, only twist values in *syn* to *anti* steps are different from the values in *anti* to *syn* steps. Other structural parameters are more or less similar in both the steps. In the case of both AP-Na and AP-K structures, *syn* to *anti* step has a lower twist value (24.6º for AP-Na and 23.6º for AP-K) than the *anti* to *syn* step (31.3º for AP-Na and 30.8º for AP-K), as in the starting structure, as well as in the crystal structure (20). Both "twist" and "slide" values are slightly smaller in the MD average structures as compared to the crystal structure. "Tilt" and "shift" values in AP-Na and AP-K,

Table IV

Average inter and intra basepair parameters, C1′ cylinder radius ($r_{C1'}$), phosphate cylinder radius (r_P) and groove width in the crystal structure (20) are listed along with the values for both the MD average 7-mer quadruplex structures (over 100-1100 ps). The parameters have been calculated taking the four strands pairwise and their standard deviation values are given within parentheses. Rotational parameters are in degrees and translational parameters are in Å units.

	Crystal	AP-Na	AP-K
Tilt	-1.1	0.1	-0.6
	(6.6)	(2.0)	(1.6)
Roll	0.0	2.7	2.6
	(6.6)	(2.6)	(2.1)
Twist	27.8[a] 33.9[b]	24.6[a] 31.3[b]	23.6[a] 30.8[b]
	(5.0) (3.3)	(1.4) (1.7)	(1.0) (1.4)
Shift	-0.3	0.0	-0.1
	(0.8)	(0.3)	(0.2)
Slide	-2.3	-1.9	-1.9
	(0.9)	(0.5)	(0.3)
Rise	3.4	3.5	3.6
	(0.4)	(0.1)	(0.1)
Propeller	-2.0	-0.5	-2.4
Twist	(12.9)	(4.6)	(3.5)
Buckle	3.5	3.1	-1.1
	(10.3)	(5.5)	(4.2)
$r_{C1'}$	8.0	7.5	7.7
	(1.3)	(0.4)	(0.3)
r_P	11.1	10.9	11.2
	(0.7)	(0.4)	(0.3)
Groove	7.1 12.3	6.5 13.3	7.0 13.0
width[c]	(0.5) (0.6)	(0.4) (0.6)	(0.7) (1.0)

[a]*Syn-Anti* step

[b]*Anti-Syn* step

[c]Groove width or shortest P--P separation on neighbouring strands corresponds to distance between phosphates separated by two guanine tetrads. The antiparallel structures have two such distances corresponding to the two different grooves.

as well as in crystal structure are close to zero whereas small positive roll is observed in both the MD average structures. Propeller twist and buckle values in both the MD average structures are comparable whereas phosphate cylinder radius (r_p), C1′ cylinder radius ($r_{C1'}$) and P--P distance across the smaller groove, all become larger in K^+ ion coordinated structure and are close to the crystal structure values. However, G-quadruplex stem in the crystal structure shows much larger variability than the MD average AP-Na and AP-K structures (as indicated by standard deviation values in Table IV).

Comparison with Other Studies

X-ray (20) and nmr (33,41) studies on *Oxytricha* telomeric sequence, $G_4T_4G_4$ demonstrated that the sequence adopts antiparallel hairpin structure with guanine residues in alternating *syn* and *anti* orientation along a strand. However, X-ray structure with potassium salt showed Greek key type folding with antiparallel adjacent strands whereas nmr structure showed Indian key topology with antiparallel diagonal strands. In the electron density map of 2.5Å crystal structure (20), one peak is observed in the center of the four guanine bases between tetrads 2 and 3 and it is interpreted as K^+ ion which can be coordinated with eight guanine O6 atoms. In our simulations, we have placed Na^+ or K^+ ions at all available sites between the tetrads, as seen in the high resolution crystal structure of parallel quadruplex (21) and recent nmr studies (41,48). This probably accounts for the antiparallel quadruplex structures in our simulations being much more uniform than the G-stem of the antiparallel crystal structure, which is also likely to be affected by crystal packing interaction. The rms deviation between the middle four nucleotides (3rd, 4th,

5th and 6th nucleotides) in the MD average AP-Na and AP-K structures is 0.81Å while the rms deviations between the 4-mer G-stem in the crystal structure (20) and middle four nucleotides (3rd, 4th, 5th and 6th nucleotides) in the MD average AP-Na and AP-K structures are 1.58Å and 1.57Å respectively. However, the rms deviation between the G-tetrads alone, in the K^+ ion coordinated crystal structure (20) and middle four G-tetrads of MD average AP-Na structure is marginally larger than the rms deviation between the G-tetrads in the crystal structure (20) and AP-K structure (1.34Å and 1.27Å respectively). The large deviation from the crystal structure is partly due to the terminal tetrad in the crystal structure taking up an all-*anti* conformation, rather than alternating *anti-syn* pattern within a tetrad. However, these deviations are comparable to the rmsd values observed within the ensemble of nmr refined structures (41) and those observed for MD average parallel structures (52) and X-ray crystal structure.

Interestingly, average hydrogen bonds and O6—O6 distances in AP-K structure are close to their average values in crystal structure (with potassium salt) whereas corresponding distances in AP-Na structure deviate more (as seen from the average hydrogen bonds and O6—O6 distances for crystal, AP-Na and AP-K structures in Table IA-B). In case of K^+ ion coordinated antiparallel quadruplex structure, the middle G-tetrad is stabilized by a cyclic single hydrogen bond pattern whereas Na^+ ion coordinated structure is mainly stabilized by three centered hydrogen bonds, suggesting a weaker paring within the G-quartet in the presence of the larger K^+ ions, in agreement with experimental data. Our earlier MD studies on 7-mer parallel G-quadruplex structures (49,52) and MD studies (50) by Spackova *et. al*. on parallel as well as antiparallel 4-mer quadruplex structures, with coordinated Na^+ ion, also indicated the presence of three centered hydrogen bonds within a G-tetrad. The MD simulation of antiparallel d($G_4T_4G_4$) Greek key type quadruplex structure (50) with Na^+ and K^+ ions (crystal coordinates as starting model) have also shown that rms deviation (with respect to initial structure) of K^+ ions coordinated structure is less than that of Na^+ ion coordinated structure. As mentioned above, the rms deviation between the G4 stem of crystal structure (20) and the middle four tetrads in MD average AP-Na and AP-K structures is around 1.6 Å, which is smaller than the rms deviation (1.9 Å) observed by Spackova et al. (50), even though they started from the crystal structure while in our studies the initial 7-mer structure corresponds to a model built structure, probably due to larger distortions at the terminii of these shorter quadruplexes during MD. Furthermore, Spackova *et al*. (50) do not report any movement of coordinated Na^+ ions through the central channel during their simulation on antiparallel Greek key type d($G_4T_4G_4$) crystal structure.

The effect of sodium, potassium and ammonium ions on the quadruplex structure formed by dimers of d($G_4T_4G_4$), with diagonal T_4 loop, has been demonstrated by a recent nmr study (41). The differences in nmr signals in Na^+ and K^+ ion coordinated structures are attributed mainly to the differences in the conformation of T_4 loops. However, in agreement with our MD studies, nmr and MD analysis of d$(G_3T_4G_3)_2$ quadruplex structure (48) demonstrated that K^+ ion coordinated quadruplex structure has fewer inter residue G(H8)-G(H8) NOESY contact and larger quadruplex diameter, when compared to Na^+ ion stabilized structure, which gets reflected in the hydrogen bond orientation and strength within G-tetrads.

The origin of ion selectivity by the guanine quadruplex structure has been investigated by several studies. Earlier gel electrophoresis studies (4,5,28,37) demonstrated that among alkali metal cations, K^+ ion exhibits optimal stereochemical fit to the cavity formed by the successive G-quartets. Similarly, nmr studies (44,45) have directly shown that K^+ ion is preferentially bound by G-quartets with respect to smaller Na^+ ion and larger Rb^+ ion. However, Hud et al. (39) argued that preferred coordination of K^+ ion over Na^+ ion is driven by the higher desolvation energy required to desolvate Na^+ ions as compared to K^+ ions. Our earlier (52) and present MD simulations have demonstrated that the coordinated K^+ ion produces larger in-plane rotational motion of guanine bases in the middle G-tetrads. Consequently average intra tetrad interaction energy between guanine bases and

stacking energy values for middle guanine tetrads in the AP-Na structure is more favourable than the corresponding values in the AP-K structure. However, the hydration free energy of K^+ ion coordinated quadruplex structure is more favourable than Na^+ ion coordinated antiparallel structure, indicating that the observed preference of K^+ ion might arise due to both factors, the greater energetic cost of Na^+ ion dehydration as well as better hydration free energy of K^+ ion coordinated structure.

The present MD study shows transient in-plane coordination of coordinated Na^+ ions which essentially allows movement of Na^+ ions along the central quadruplex axis, while larger K^+ ions are relatively stationary and occupy the coordination sites between two G-tetrads. However, at 400K, we do observe movement of the coordinated K^+ ion at the 3′ end of the quadruplex, but this leads to a disruption of the 3′ terminal G-tetrad. Several nmr studies (44,47) have also demonstrated the free movement of Na^+ ions (ionic radius 0.95 Å) through the quadruplex channel, whereas coordinated NH_4^+ ions (ionic radius 1.43 Å), which are comparable in size to K^+ ions (ionic radius 1.33 Å) show quite high residence time (47). A preliminary 400ps MD study on a 7-mer Indian key type antiparallel quadruplex structure (unpublished data) shows similar movement of coordinated Na^+ ion through the quadruplex channel. The middle G-tetrads in the Indian key type structure also adopt bifurcated hydrogen bonds, similar to that observed in the present study on Greek key type AP-Na structure, while still retaining the characteristic groove dimensions of the Indian key structure i.e. one large, one small and two medium grooves. Overall the Na^+ ion-G4 stem interaction energies also appear to be nearly same in both structures, indicating that the preference for Indian key structure in solution may arise due to better interaction with the thymine loops, in the folded back structures.

Our earlier MD studies on parallel G-quadruplex structures (49,52) and present studies on antiparallel G-quadruplex structures indicate that hydrogen bonding scheme within the G-tetrad and quadruplex diameter is influenced by the size of coordinated cations. It is observed that the average base-base interaction energy within a G-tetrad is marginally more favourable in both the antiparallel structures than in the corresponding parallel structures (52). However, while the stacking energy of G-tetrads with coordinated Na^+ ions are comparable for parallel and antiparallel structures, the stacking energy for the K^+ ion coordinated parallel structure is marginally more favourable than for the antiparallel structure. In addition, as mentioned above, the estimated hydration free energy of antiparallel quadruplex structures (for both Na^+ and K^+ ions coordinated structures) is less favourable than that for the respective parallel structures. This could explain the preference of single stretches of guanines to take up the parallel structure.

Conclusions

Our MD studies have demonstrated that base interaction energy within a G-tetrad depends on the tetrad geometry, in particular on the position of the charged groups. Similarly, base-stacking energy between two successive guanine tetrads depends on orientation of O6 atoms and it is close to zero in both the AP-Na and AP-K structures. However, interaction energy between coordinated ion and G-tetrad is favourable for both the structures.

In the MD structures, strong attractive force between the coordinated Na^+ ions and guanine O6 atoms rotates the guanine bases in G-tetrads, leading to smaller O6—O6 separation and a network of bifurcated hydrogen bonds between neighbouring guanine bases, rather than the two standard Hoogsteen type hydrogen bonds, seen in the crystal structures. However, four tetrads at the two terminii of AP-K structure are stabilized by standard Hoogsteen hydrogen bonds while the middle tetrad in K^+ ion coordinated structure is stabilized only by a cyclic single hydrogen bond. The effect of the size of the coordinated ion on the quadruplex structures appears to be more pronounced for the longer fragment used in our simulation, perhaps due

to the cumulative effect of the larger number of ions present in the central cavity.

The smaller size of the coordinated Na^+ ions allows them greater mobility than the K^+ ions. The present analysis along with our earlier results on parallel quadruplexes indicates that the Na^+ ions can move through the quadruplex channel without disturbing the tetrad geometry, as well as enter or exit the quadruplex core through the quadruplex ends, indicating that not all sites in the quadruplex cavity need to be occupied for structural integrity. The coordinated K^+ ions, due to their larger size cannot easily move within the central channel and are forced out of the quadruplex cavity at higher temperature only by disrupting the G-tetrad geometry. However, the essential quadruplex nature of the structure is retained for both these longer quadruplexes, even at this higher (400K) temperature.

Na^+ counter ions, present in the solvent are most often located near the phosphate groups of quadruplex structures. However, some counter ions are also bound inside the quadruplex grooves. The two smaller grooves in Greek key type antiparallel structures are better binding sites for counter ions than the two wider grooves. In both the antiparallel structures, quite a few water molecules stay close to the guanine base atoms and form hydrogen bonds, with the exposed 2-amino groups and N3 atoms of guanines being the preferred binding sites for water molecules.

Hence, Na^+ and K^+ ions coordinated antiparallel G-quadruplexes are structurally very stable and can retain a quadruplex structure even at 400K. However, hydration free energy of antiparallel structure are noticeably less favourable than for the parallel quadruplex structures, which can explain the preference for parallel strand arrangement in quadruplex structure formed by guanine oligomers. Among the two antiparallel structures, hydration free energy for the K^+ ion coordinated structure is more favourable than the hydration free energy for the Na^+ ion coordinated structure. This along with the higher desolvation energy for a Na^+ ion could account for the observed preference for K^+ ions, as indicated by nmr experiments.

Acknowledgement

This work is partially supported by a grant from CSIR, INDIA. The authors are grateful to SERC, I. I. Sc., for computational facilities.

References and Footnotes

1. M. Gellert, M.N. Lipsett and D.R. Davies, *Proc. Natl. Acad. Sci. U.S.A. 48*, 2013-2018 (1962).
2. W. Guschlbauer, J.F. Chantot and D.J. Thiele, *J. Biomol. Struct. Dyn. 8*, 491-511 (1990).
3. T.R. Cech, *Nature 332*, 777-778 (1988).
4. W.I. Sundquist and A. Klug, *Nature 342*, 825-829 (1989).
5. J.R. Williamson, M.K. Raghuraman and T.R. Cech, *Cell 59*, 871-880 (1989).
6. E. Blackburn, *Nature 350*, 569-573 (1991).
7. D. Sen and W. Gilbert, *Nature 334*, 364-366 (1988).
8. A.I.H. Murchie and D.M.J. Lilley, *Nucl. Acids Res. 20*, 49-53 (1992).
9. K. Walsh and A. Gualberto, *J. Bio. Chem. 267*, 13714-13718 (1992).
10. W.I. Sundquist and S. Heaphy, *Proc. Natl. Acad. Sci. U.S.A. 90*, 3393-3397 (1993).
11. A. Kettani, R.A. Kumar and D.J. Patel, *J. Mol. Biol. 254*, 638-656 (1995).
12. J.R. Williamson, *Curr. Opin. Struct. Biol. 3*, 357-362 (1993).
13. J.R. Williamson, *Annu. Rev. Biophys. Biomol. Struc. 23*, 703-730 (1994).
14. G. Fang and T.R. Cech, *Biochemistry 32*, 11646-11657(1993).
15. P. W. Shomer and M. Fry, *J. Biol. Chem. 268*, 3306-3312 (1993).
16. K.Y. Wang, S.H. Krawczyk, N. Bischofberger, S. Swaminathan and P.H. Bolton, *Biochemistry 32*, 11285-11292 (1993).
17. R. Giraldo and D. Rhodes, *EMBO J. 13*, 2411-2420 (1994).
18. S. Arnott, R. Chandrasekaran and C.M. Marttila, *Biochem. J. 141*, 537-543 (1974).
19. S. B. Zimmerman, G.H. Cohen and D.R. Davies, *J. Mol. Biol. 92*, 181-192 (1975).
20. C. Kang, X. Zhang, R. Ratliff, R. Moyzis and A. Rich, *Nature 356*, 126-131 (1992).
21. K. Phillips, Z. Dauter, A.I.H. Murchie, D.M.J. Lilley and B. Luisi, *J. Mol. Biol. 273*, 171-182 (1997).
22. D. Mohanty and M. Bansal, *Nucl. Acids Res. 21*, 1767-1774 (1993).
23. D. Mohanty and M. Bansal, *Biopolymers 34*, 1187-1211 (1994).

24. D. Mohanty and M. Bansal, *Biophys. J. 69*, 1046-1067 (1995).
25. P. Balagurumoorthy, S.K. Brahmachari, D. Mohanty, M. Bansal, and V. Sasisekharan, *Nucl. Acids Res. 20*, 4061-4067 (1992).
26. J. Kim, C. Cheong and P.B. Moore, *Nature 351*, 331-332 (1991).
27. F. Aboul-ela, A.I.H. Murchie and D.M.J. Lilley, *Nature 360*, 280-282 (1992).
28. C.C. Hardin, E. Henderson, T. Watson and J.K. Prosser, *Biochemistry 30*, 4460-4472 (1991).
29. C.C. Hardin, T. Watson, M. Corregan, C. Bailey, *Biochemistry 31*, 833-841 (1992).
30. T. Miura and G.J. Thomas Jr, *Biochemistry 34*, 9645-9654 (1995).
31. G. Gupta, A.E. Garcia, Q. Guo, M. Lu and N.R. Kallenbach, *Biochemistry 32*, 7098-7103 (1993).
32. Y. Wang, C.D.L. Santos, X. Gao, K. Greene, D. Live and D.J. Patel, *J. Mol. Biol. 222*, 819-832 (1991).
33. F.W. Smith and J. Feigon, *Nature 356*, 164-168 (1992).
34. P. Schultze, R.F. Macaya, F.W. Smith, J.A. Roe and Feigon, J. *Proc. Natl. Acad. Sci. U.S.A. 90*, 3745-3749 (1993).
35. K. Padmanabhan, K.P. Padmanabhan, J.D. Ferrara, J.E. Sadler and A. Tulinsky, *J. Biol. Chem. 268*, 17651-17654 (1993).
36. P. Balagurumoorthy and S.K. Brahmachari, *J. Biol. Chem. 269*, 21858-21869 (1994).
37. D. Sen and W. Glibert, *Nature 344*, 410-414 (1990).
38. T. Miura, J.M. Benevides and G.J. Thomas Jr., *J. Mol. Biol*. 248, 233-238 (1995).
39. N.V. Hud, F.W. Smith, F.A.L. Anet and J. Feigon, *Biochemistry 35*, 15383-15390 (1996).
40. V.M. Marathias and P.H. Bolton, *Biochemistry 38*, 4355-4364 (1999).
41. P. Schultze, N.V. Hud, F.W. Smith and J. Feigon, *Nucl. Acids Res. 27*, 3018-3028 (1999).
42. W. Ross and C.C. Hardin, *J. Am. Chem. Soc. 116*, 6070-6080 (1994).
43. P.V. Scaria, S.J. Shire and R.H. Shafer, *Proc. Natl. Acad. Sci. U.S.A. 89*, 10336-10340 (1992).
44. Q. Xu, H. Deng and W. H. Braunlin, *Biochemistry 32*, 13130-13137 (1993).
45. H. Deng and W.H. Braunlin, *J. Mol. Biol. 255*, 476-483 (1996).
46. C.C. Hardin, M.J. Corregan, D.V. Lieberman and B.A. Brown II, *Biochemistry 36*, 15428-15450 (1997).
47. N.V. Hud, P. Schultze, V. Sklenar and J. Feigon, *J. Mol. Biol. 285*, 233-243 (1999).
48. G.D. Strahan, M.A. Keniry and R.H. Shafer, *Biophys. J. 75*, 968-981 (1998).
49. M. Bansal, M. Ravikiran and S. Chowdhury, Computational Molecular Biology; (Edited by J. Leszczynski), Elsevier Science, 279-323 (1999).
50. N. Spackova, I. Berger, and J. Sponer, *J. Am. Chem. Soc. 121*, 5519-5534 (1999).
51. J. Gu, J. Leszczynski and M. Bansal, *Chem. Phys. Letters 311*, 209-214 (1999).
52. S. Chowdhury and M. Bansal, *J. Biomol. Struct. Dyn. 18*, 11-28 (2000).
53. W.L. Jorgensen, J. Chandresekher, J. Madura, R.W. Impey and M.L. Klein, *J. Chem. Phys. 79*, 926-937 (1983).
54. W.D. Cornell, P. Cieplak, C.L. Bayly, I.R. Gould, K.M. Merz Jr., D.M. Ferguson, D.C. Spellmeyer, T. Fox, J.W. Caldwell and P.A. Kollman, *J. Am. Chem. Soc. 117*, 5179-5197 (1995).
55. T. Darden, D. York and L. Pedersen, *J. Chem. Phys. 98*, 10089-10092 (1993).
56. T. E. Cheatham, J. L. Miller, T. Fox, T. Darden and P. A. Kollman, *J. Am. Chem. Soc. 117*, 4193-4194 (1995).
57. H. Lee, T. Darden and L. Pedersen, *J. Chem. Phys. 102*, 3830-3834 (1995).
58. T. Darden, L. Perera, L. Li and L. Pedersen, *Structure 7*, 55-60 (1999).
59. M.A. Young, B. Jayaram and D.L. Beveridge, *J. Phys. Chem. B 102*, 7666-7669 (1998).
60. Y. Duan, P. Wilkosz, M. Crowley and J.M. Rosenberg, *J. Mol. Biol. 272*, 553-572 (1997).
61. M. Feig and B.M. Pettitt, *Biophys. J.* 77, 1769-1781 (1999).
62. T.E. Cheatham III, P. Cieplak and P.A. Kollman, *J. Biomol. Struct. Dyn. 16*, 845-862 (1999).
63. D. Bhattacharyya and M. Bansal, *J. Biomol. Struct. Dyn. 6*, 635-653 (1989).
64. M. Bansal, D. Bhattacharyya and B. Ravi, *CABIOS 11*, 281-287 (1995).
65. K.J. Edwards, D.G. Brown, N. Spink, J.V. Skelly and S. Neidle, *J. Mol. Biol. 226*, 1161-1173 (1992).
66. M.S. Lopez, L. Malinina, J. Lie, T.H. Dinh and J.A. Subirana, *J. Biol. Chem. 274*, 23683-23686 (1999).
67. M.A. Young, G. Ravishanker and D.L. Beveridge, *Biophys. J. 73*, 2313-2336 (1997).
68. B. Schneider, D.M. Cohen, L. Schleifer, A.R. Srinivasan, W.K. Olson and H.M. Berman, *Biophys. J. 65*, 2291-2303 (1993).
69. M.L. Connolly, *Science 221*, 709-713 (1983).
70. M.L. Connolly, *J. Mol. Graphics 11*, 139-141 (1993).
71. D. Eisenberg and A.D. MacLachlan, *Nature 319*, 199-203 (1986).
72. T.F. Kagawa, D. Stoddard, G. Zhou and P.S. Ho, *Biochemistry 28*, 6642-6651 (1989).
73. T.F. Kagawa, M.L. Howell, K. Tseng and P.S. Ho, *Nucl. Acids Res. 21*, 5978-5986 (1993).

Date Received: September 6, 2000

Communicated by the Editor Wolfram Saenger